

The metabolite alpha-ketobutyrate extends lifespan by promoting peroxisomal function in *C. elegans*

Received: 21 February 2022

Accepted: 6 January 2023

Published online: 16 January 2023

 Check for updatesNan Wu^{1,2}, Yi-Cheng Ma^{1,2}, Xin-Qian Gong^{1,2}, Pei-Ji Zhao ^{1,2}, Yong-Jian Jia¹, Qiu Zhao¹, Jia-Hong Duan¹ & Cheng-Gang Zou ¹✉

Metabolism is intimately linked to aging. There is a growing number of studies showing that endogenous metabolites may delay aging and improve healthspan. Through the analysis of existing transcriptome data, we discover a link between activation of the transsulfuration pathway and a transcriptional program involved in peroxisome function and biogenesis in long-lived *glp-1(e2141ts)* mutant *Caenorhabditis elegans* worms. Subsequently, we show that supplementation with α -ketobutyrate, an intermediate of the transsulfuration pathway, extends lifespan in wild-type worms. Alpha-ketobutyrate augments the production of NAD^+ via the lactate dehydrogenase LDH-1, leading to SIR-2.1/SIRT1-mediated enhanced peroxisome function and biogenesis, along with a concomitant increase in the expression of *acox-1.2/ACOX1* in the peroxisomal fatty acid β -oxidation pathway. ACOX-1.2/ACOX1 promotes H_2O_2 formation, thereby resulting in activation of SKN-1/NRF2. This transcription factor in turn extends the lifespan of worms by driving expression of autophagic and lysosomal genes. Finally, we show that α -ketobutyrate also delays the cellular senescence in fibroblast cells through the SIRT1-ACOX1- H_2O_2 -NRF2 pathway. This finding uncovers a previously unknown role for α -ketobutyrate in organismal lifespan and healthspan by coordinating the NAD^+ -SIRT1 signaling and peroxisomal function.

The transsulfuration pathway (TSP) is an evolutionarily conserved pathway that commits methionine to cysteine synthesis in metazoan^{1–3}. There are two key enzymes, cystathionine β -synthase (CBS) and cystathionase (CTH, also called cystathionine γ -lyase, GCL), in this pathway. CBS converts serine and homocysteine into cystathionine, while CTH catalyzes the elimination of cystathionine to form cysteine and α -ketobutyrate (α -KB)^{1,2}. Both CBS and CTH catalyze the production of a gas hydrogen sulfide (H_2S) via condensation of cysteine and homocysteine, and desulfhydration of cysteine, respectively^{2,4}. In the fruit fly *Drosophila melanogaster* and the nematode *Caenorhabditis elegans*, overexpression of CBS extends lifespan, which is probably due to increased H_2S production^{4,5}. As a product of

TSP, H_2S can function as a signaling molecule to extend lifespan and improve healthspan^{4,6,7}. Although the underlying mechanism remains unknown, supplementation with NaHS, a compound that can produce H_2S , increases the NAD^+ levels in mammalian cells⁸. It has been well-established that elevation of intracellular NAD^+ levels by supplementation of NAD^+ precursors such as nicotinamide mononucleotide (NAM) and nicotinamide mononucleotide (NMN), or activation of the de novo NAD^+ synthesis pathway, promotes healthspan and extends lifespan via a mechanism requiring SIRT1/SIR-2.1 across species from worms to mammals^{9–12}. However, the role of α -KB, another product of TSP, in the regulation of longevity remains unknown.

¹State key Laboratory for Conservation and Utilization of Bio-Resources in Yunnan, School of Life Sciences, Yunnan University, Kunming, Yunnan 650091, China. ²These authors contributed equally: Nan Wu, Yi-Cheng Ma, Xin-Qian Gong, Pei-Ji Zhao. ✉e-mail: chgrou@ynu.edu.cn

In *C. elegans*, *glp-1* encodes a Notch receptor crucial for the regulation of the germline stem cell pool¹³. The germline can be removed by blocking germline stem-cell proliferation with the temperature-sensitive (ts) *glp-1(e2144ts)* mutation^{14,15}. The germ-cell loss extends *C. elegans* lifespan through activating transcription factors such as DAF-16/FOXO and SKN-1/NRF2 and nuclear hormone receptors such as DAF-12 and NHR-80^{14–22}. Interestingly, the levels of H₂S production are also elevated, which is mediated by reactive oxygen species (ROS) derived from mitochondria, in the germline-deficient *glp-1(e2141ts)* mutants. H₂S promotes the nuclear translocation of SKN-1, thereby extending lifespan in the germline-deficient worms¹⁵. Besides *glp-1(e2141ts)* mutants, ROS levels are elevated in respiration mutants, such as *clk-1(qm30)*, *isp-1(qm150)*, and *nuo-6(qm200)* mutants, which are responsible for longevity extension by increasing the activity of hypoxia-inducible factor HIF-1^{23,24}. Meanwhile, lifespan is extended in response to increased levels of ROS through treatment with 2-deoxyglucose or a low dosage of the oxidant paraquat in worms^{25–27}. These data suggest that ROS act as signaling molecules to regulate lifespan.

By analyzing existing transcriptome data of long-lived *glp-1(e2141ts)* mutants in two independent studies (GSE43864 and GSE63075)^{20,28}, we observed an upregulation of a set of peroxisome-related genes, which are involved in peroxisomal biogenesis, peroxisomal fatty acid β -oxidation, and amino acid metabolism. These data implicate a role of enhanced peroxisomal function in lifespan extension in germline-deficient worms. As a representative of highly plastic organelles, peroxisomes are capable of modifying their size, abundance, and morphology in response to cellular or environmental cues²⁹. The peroxisome has been implicated in aging and longevity regulation^{30–33}, yet the exact role and mechanism of action of peroxisome in longevity are far from fully elucidated.

In this study, we demonstrated that the levels of α -KB, another product of TSP, were elevated in germline-deficient *glp-1(e2141ts)* mutants. Supplementation with α -KB promoted peroxisome biogenesis, leading to an increase in H₂O₂ production, in an NAD⁺-SIRT1 signal-dependent manner. H₂O₂, in turn, induced autophagy via SKN-1/NRF2, thereby extending lifespan in the germline-deficient animals. Finally, our data demonstrated that α -KB treatment reduced cellular senescence in mammalian cells. These findings provide novel pharmacological approaches to prevent age-related physiological decline.

Results

Alpha-KB extends the lifespan in worms

We analyzed the transcriptome data of *glp-1(e2141ts)* mutants in two independent studies^{20,28}, and identified that there were 3208 overlapped genes upregulated between the two datasets (Supplementary Fig. 1a), including the major genes in TSP, such as *cth-1*, *cth-2*, and *cbs-1* (Supplementary Fig. 1b). These results implicate that TSP is activated in germline-deficient worms. To assess whether TSP is activated in germline-deficient *glp-1(e2141ts)* mutants, we first determined the expressions of *cbs-1*, *cth-1*, and *cth-2*, the major genes in TSP^{4,7}. Using qPCR, we found that the expressions of *cth-1*, and *cth-2*, but not *cbs-1*, were markedly upregulated in germline-deficient animals (Fig. 1a). Previously, we developed a fluorescent chemodosimeter for monitoring endogenous H₂S in mammalian cells, flies and worms³⁴. Using the fluorescent probe, we found that the relative levels of H₂S were significantly increased in germline-deficient animals (Fig. 1b, c), which was consistent with a previous study¹⁵. These data suggest that TSP is activated in germline-deficient worms. We then asked whether another product of TSP, α -KB, which is derived from the elimination of cystathionine catalyzed by CTH^{2,3}, was elevated in these animals. Using LC-MS, we found that the levels of α -KB were significantly increased in germline-deficient mutants, compared with those in wild-type (WT) worms (Fig. 1d). RNAi knockdown of

either *cth-1* or *cth-2* reduced the levels of α -KB in germline-deficient worms back to those of WT worms (Fig. 1d).

A previous study has demonstrated that the knockdown of *cth-2* does not affect the lifespan of WT animals³⁵. Likewise, the *cth-1(ok3319)* mutants do not exhibit an overall significantly shorter maximal lifespan although these animals initially display a much higher death rate³⁶. Consistent with these observations, we found that RNAi knockdown of either *cth-1* or *cth-2* did not alter the lifespan of WT worms (Supplementary Fig. 2a, b and Supplementary Data 1). However, RNAi knockdown of either *cth-1* or *cth-2* shortened the lifespan of germline-deficient worms (Supplementary Fig. 2a, b). Although supplementation with α -KB did not further extend the lifespan of germline-deficient worms, it partially restored the lifespan of germline-deficient worms subjected to *cth-1* or *cth-2* RNAi (Supplementary Fig. 2a, b). In addition, we determined the effect of α -KB supplementation on lifespan in other three longevity pathways: DR (the feeding deficient mutant *eat-2*), reduced insulin/IGF-1 signaling (the receptor mutant *daf-2*), reduced mitochondrial respiration (the mitochondrial complex III mutant *isp-1*). We found that supplementation with α -KB could extend the lifespan of *eat-2(ad1116)*, but not *isp-1(qm150)* and *daf-2(e1370)* (Supplementary Fig. 3a–c and Supplementary Data 1).

Considering both CTH-1 and CTH-2 are H₂S-producing enzymes^{1,2}, we tested the combined effects of α -KB and H₂S. Like α -KB, supplementation with NaHS (300 μ M) also partially restored the lifespan of *glp-1(e2141ts)* mutants subjected to either *cth-1* or *cth-2* RNAi (Supplementary Fig. 2a, b). However, supplementation with both α -KB and NaHS did fully restore the lifespan of *glp-1(e2141ts)* mutants subjected to either *cth-1* or *cth-2* RNAi (Supplementary Fig. 2a, b). These results indicate that the upregulation of either *cth-1* or *cth-2* contributes to lifespan extension in *glp-1(e2141ts)* mutants via both α -KB and H₂S.

Next, we investigated the effect of α -KB in WT worms and found that supplementation with α -KB significantly extended the lifespan of WT worms (Fig. 1e and Supplementary Data 1). Moreover, we determined the effect of α -KB on several age-associated markers, pharyngeal-pumping rate, body bending, lipofuscin autofluorescence^{37,38}, the integrity of intestinal barrier, and aggregation of polyglutamine::YFP (Poly-Q35::YFP)³⁹. As expected, the reduction in both pharyngeal-pumping rate (Fig. 1f) and body bending (Fig. 1g) in 8-day-old worms was significantly inhibited after α -KB treatment. We detected the integrity of the intestinal barrier using food dye FD&C Blue No. 1, and found that the body-cavity leakage in 10-day-old worms treated with α -KB than that in age-matched worms with vehicle (Fig. 1h, i). In contrast, supplementation with α -KB did not affect the number of Poly-Q35::YFP aggregates in body wall muscle cells of 8-day-old worms (Supplementary Fig. 4a, b). Taken together, these results suggest that α -KB treatment delays the aging process in worms.

Lifespan extension involves NAD⁺ production in a SIR-2.1-dependent fashion

Increased oxidized nicotinamide adenine dinucleotide (NAD⁺) levels improve lifespan and healthspan across species, including worms^{10,11,40–42}. α -KB is readily reduced via lactate dehydrogenase or other intracellular dehydrogenases to generate NAD⁺^{43,44}. Indeed, using LC-MS, we found that supplementation with α -KB increased the NAD⁺ levels in WT worms (Fig. 2a). Knockdown of either *cth-1* or *cth-2* by RNAi reduced the levels of NAD⁺ in WT worms, which were restored by supplementation with α -KB. Furthermore, an increase in the NAD⁺ levels was observed in *glp-1(e2141ts)* mutants (Fig. 2a). Knockdown of either *cth-1* or *cth-2* by RNAi reduced the levels of NAD⁺ in germline-deficient worms back to those of WT worms (Fig. 2a).

The beneficial effects of NAD⁺ on lifespan extension depend on SIR-2.1 (the *C. elegans* ortholog of SIRT1), a member of the sirtuin family of NAD⁺-dependent deacylases^{10,11,41,42}. We then asked whether SIR-2.1 was involved in α -KB-mediated lifespan extension. RNAi knockdown of *sir-2.1* completely blocked lifespan extension by α -KB

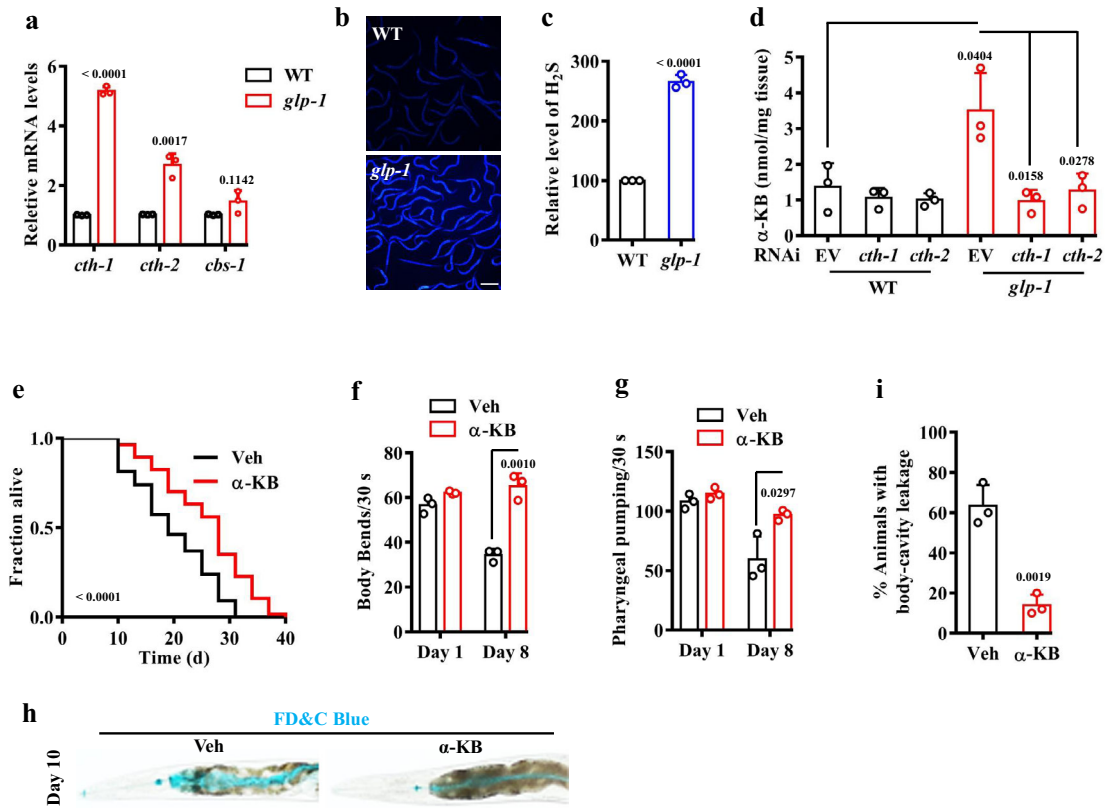


Fig. 1 | Alpha-KB promotes lifespan in worms. **a** The mRNA levels of *cth-1* and *cth-2*, but not *cbs-1*, were upregulated in *glp-1(e2141ts)* mutants, compared with those in wild-type (WT) worms. These results are means \pm SD of three independent experiments. **b**, **c** Representative images of H₂S formation detected by a fluorescent probe. A similar pattern of H₂S formation was observed in three independent experiments. Scale bars: 500 μ m. **c** Quantification of fluorescent intensity in **b**. The content of H₂S was increased in *glp-1(e2141ts)* mutants, compared with that in WT worms. Data were presented as mean values \pm SEM of three independent experiments ($n = 35$ worms per experiment). *P* values (**a**, **c**) were calculated using the two-sample *t*-test. **d** The levels of α -ketobutyrate (α -KB) were increased in *glp-1(e2141ts)* mutants, compared with that in WT worms. RNAi knockdown of either

cth-1 or *cth-2* reduced the contents of α -KB in *glp-1(e2141ts)* mutants back to those of WT worms. Data were presented as mean values \pm SEM of three independent experiments. **e** Supplementation with α -KB (500 μ M) extended lifespan in WT worms. Veh vehicle. *P* value was calculated using a log-rank test. See survival statistics in Supplementary Data 1. **f–i** Supplementation with α -KB delayed the appearance of the aging markers, including pharyngeal pumping (**f**), body bending (**g**), and body-cavity leakages (**h**, **i**) in WT worms. Scale bars: 500 μ m. Data were presented as mean values \pm SEM of three independent experiments ($n = 25$ worms per experiment). *P* values (**d**, **f**, **g**, **i**) were calculated using a one-way ANOVA followed by a Student–Newman–Keuls test. Source data are provided as a Source Data file.

treatment (Fig. 2b and Supplementary Data 1) but only partially reduced lifespan extension by the *glp-1(e2141ts)* mutation (Supplementary Fig. 5 and Supplementary Data 1). Thus, SIR-2.1 is specifically required for α -KB-mediated lifespan extension. By contrast, SIR-2.1 is not specific to longevity in *glp-1(e2141ts)* mutants. Taken together, these results suggest that α -KB extends the lifespan by increasing NAD⁺ levels and its effect depends on the concomitant activity of SIR-2.1.

Alpha-KB stimulates peroxisome biogenesis and function

As mentioned above, we compared with the expression profiles of *glp-1(e2141ts)* mutants from two previous transcriptomic studies^{20,28} (Supplementary Fig. 1a). From the overlapping genes from those two studies, both KEGG pathway and Gene Ontology enrichment analyses revealed that one of the top five overrepresented categories was “peroxisome” (Supplementary Fig. 1c). The “peroxisome” genes included peroxins (PEXs) required for peroxisomal protein import and proliferation (e.g., *prx-1*, *-2*, *-3*, *-5*, *-11*, *-12*, and *-19*)⁴⁵, and peroxisomal genes required for fatty acid beta-oxidation (e.g., *acox-1.1*, *-1.2*, *-1.3*, *-1.4*, *-1.5*, *-1.6*, *-3*, *acs-2*, *-5*, *-13*, *-16*, *-17*, and *dhs-28*) (Supplementary Fig. 1d). These results suggest that germline removal probably enhances peroxisome biogenesis. To monitor whether peroxisome number and size were altered, we used a *C. elegans* peroxisome reporter in which mRFP was linked to a peroxisome-targeting sequence (PTS1) under control by an intestinal promoter (*vha-6p::mRFP-PTS1*)³¹. Confocal images were taken

from the Int1 and Int2 cells (the first two anterior rings of the intestine) (Supplementary Fig. 6a). We found that germline-deficient animals displayed an increase in the abundance of mRFP puncta over WT animals (Fig. 3a, b). Meanwhile, the size of peroxisomes also increased in germline-deficient animals (Supplementary Fig. 6b). It should be noted that the punctate pattern was not observed in non-fluorescent strains (Supplementary Fig. 6a). RNAi knockdown of either *cth-1* or *cth-2* reduced the number and size of peroxisomes in *glp-1(e2141ts)* mutants back to those of WT worms (Fig. 3a, b and Supplementary Fig. 6b). Although supplementation with α -KB did not influence the number and size of peroxisomes in germline-deficient animals, it significantly restored the number and size of peroxisomes in these animals subjected to *cth-1* or *cth-2* RNAi (Fig. 3a, b and Supplementary Fig. 6b). Meanwhile, the number and size of peroxisomes were considerably increased in WT worms treated with α -KB (Fig. 3c, d and Supplementary Fig. 6c).

Although PTS1-labeled marker proteins, such as mRFP-PTS1 or GFP-SKL, have been used to determine the number and size of peroxisomes^{31,46}, they actually represent peroxisomal import function³¹. We thus determined the number and size of peroxisomes using transgenic worms expressing *pmp-2p::pmp-2::mCherry*. PMP-2, the *C. elegans* homolog of mammalian PMP70, is a peroxisomal membrane protein⁴⁶. We observed that both the number and size of peroxisomes were increased in both *glp-1(e2141ts)* mutants and α -KB-

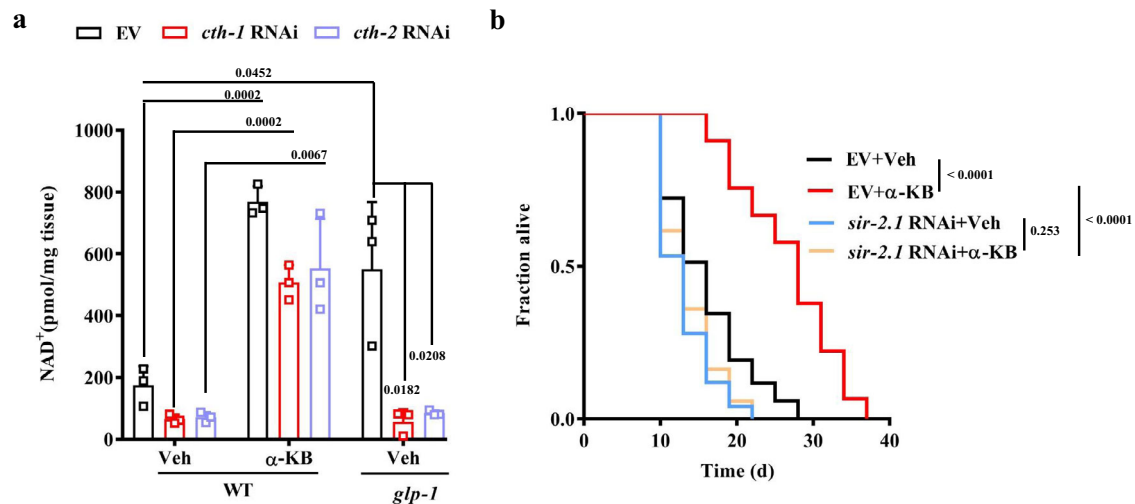


Fig. 2 | Lifespan extension by α -KB depends on the NAD⁺-SIR-2.1 pathway. **a** The contents of NAD⁺ were increased in α -ketobutyrate (α -KB, 500 μ M)-treated wild-type (WT) worms or *glp-1(e214ts)* mutants. Knockdown of either *cth-1* or *cth-2* by RNAi reduced the levels of NAD⁺ in germline-deficient worms back to those of WT worms. Veh vehicle. Data were presented as mean values \pm SEM of three

independent experiments. *P* value was calculated using a one-way ANOVA followed by a Student–Newman–Keuls test. **b** RNAi knockdown of *sir-2.1* inhibited lifespan extension by α -KB (500 μ M) in WT worms. *P* values were calculated using a log-rank test. See survival statistics in Supplementary Data 1. Source data are provided as a Source Data file.

treated worms expressing *pmp-2p::pmp-2::mCherry* (Supplementary Fig. 7a–f). As PEX11 in yeast and mammals is involved in peroxisomal division and proliferation, we also determined the effect of α -KB on the number and size of peroxisomes by measuring the expression of *prx-11p::prx-11::gfp*, the *C. elegans* homolog of PEX11. We found that both the number and size of peroxisomes were increased in α -KB-treated worms expressing *prx-11p::prx-11::gfp* (Supplementary Fig. 8a–c). These results suggest that elevated α -KB levels via upregulation of *cth-1* and *cth-2* in *glp-1(e214ts)* mutants or supplementation with α -KB in WT worms increase the number and size of peroxisomes.

Using qPCR, we determined the expression of the peroxisome-related genes, such as *prx-2*, *prx-19*, *acox-1.2*, *acox-3*, *acs-2*, and *acs-5*. Of these genes, the expressions of these peroxisome-related genes were significantly upregulated in *glp-1(e214ts)* mutants, compared with those in WT worms (Supplementary Fig. 9a). Knockdown of *cth-1* or *cth-2* by RNAi reduced the expressions of these genes in *glp-1(e214ts)* mutants back to those of WT worms. Utilizing transgenic worms expressing *acox-1.2p::gfp*, we found that the expression of *acox-1.2p::gfp* was substantially upregulated in *glp-1(e214ts)* mutants (Fig. 3e, f). RNAi knockdown of *cth-1* or *cth-2* reduced the expression of *acox-1.2p::gfp* in *glp-1(e214ts)* mutants back to those of WT worms. This increase in the expression of *acox-1.2p::gfp* was inhibited after the knockdown of *cth-1* and *cth-2* by RNAi. Although supplementation with α -KB did not influence the expression of *acox-1.2p::gfp* in *glp-1(e214ts)* mutants, it markedly restored its expression in these animals subjected to *cth-1* or *cth-2* RNAi (Fig. 3e, f). Finally, we found that α -KB treatment significantly upregulated the expression of *acox-1.2p::gfp* and *ctl-2*, encoding a peroxisomal catalase, in WT worms (Fig. 3g, h and Supplementary Fig. 9b). Taken together, these results suggest that peroxisome biogenesis and function are promoted by α -KB.

We asked the question of whether α -KB promoted peroxisome biogenesis by the production of NAD⁺. As α -KB can produce NAD⁺ via the lactate dehydrogenase^{43,44}, we blocked the production of NAD⁺ by silencing *ldh-1*, which encoded the *C. elegans* lactate dehydrogenase. We found that knockdown of *ldh-1* by RNAi significantly inhibited the increase in the number and the size of peroxisomes (Fig. 3c, d and Supplementary Fig. 6c), and inhibited the expression of *acox-1.2p::gfp* in α -KB-treated WT worms (Fig. 3g, h). Next, knockdown of *sir-2.1* by

RNAi suppressed the increase in either the number and size of peroxisomes (Fig. 3c, d and Supplementary Fig. 6c) or the expression of *acox-1.2p::gfp* in WT worms treated with α -KB (Fig. 3g, h). In addition, we tested the roles of NAD⁺ precursors, such as NAM, NMN, and nicotinamide riboside (NR)¹². We found that supplementation with NAM, NMN, and NR considerably promoted the number and size of peroxisomes (Supplementary Figs. 10a–c, 11a–c), and upregulated the expression of *acox-1.2p::gfp* in WT worms (Supplementary Fig. 10d, e). Taken together, these results indicate that α -KB promotes peroxisome biogenesis and function by NAD⁺ and *sir-2.1*.

A previous study has demonstrated that AMP-activated protein kinase (AMPK) and caloric restriction promote longevity via remodeling mitochondrial and peroxisomal networks in worms³¹, raising the possibility that α -KB may function in mitochondria-peroxisome coordination. However, we found that α -KB did not delay the reduction in mitochondrial content with age (Supplementary Fig. 12a). Furthermore, RNAi knockdown of *aak-2*, which encodes catalytic subunits of AMPK, did not affect the lifespan of α -KB-treated WT animals (Supplementary Fig. 12b and Supplementary Data 1). More importantly, supplementation with α -KB did not affect the levels of phosphorylated AMPK(Thr172) in both worms and senescent IMR90 cells, a human lung fibroblast strain (Supplementary Fig. 12c, d). By contrast, the levels of phosphorylated AMPK(Thr172) were markedly higher in *glp-1(e214ts)* mutants than those in WT worms (Supplementary Fig. 12c). Thus, lifespan extension by α -KB is not linked to maintenance of the mitochondrial networks mediated by AMPK.

Peroxisome function and H₂O₂ production are required for α -KB-mediated lifespan extension

To determine whether the peroxisomal function is required for longevity, we silenced the peroxisomal genes, *prx-2* (the *C. elegans* homolog of mammalian peroxisome biogenesis factor 2; PEX2) and *prx-19* (the *C. elegans* homolog of mammalian peroxisome biogenesis factor 19; PEX19), which are involved in the peroxisomal import proteins⁴⁷. In WT worms treated with α -KB or vehicle, RNAi knockdown of either *prx-2* or *prx-19* severely reduced the number of peroxisomes (Supplementary Fig. 13a, b). These results indicate that mRFP fails to import into peroxisomes. Moreover, the knockdown of *prx-2* and *prx-19* by RNAi reduced the lifespan of α -KB-treated WT worms back to that of WT worms treated with vehicle (Fig. 4a, b and Supplementary Data 1).

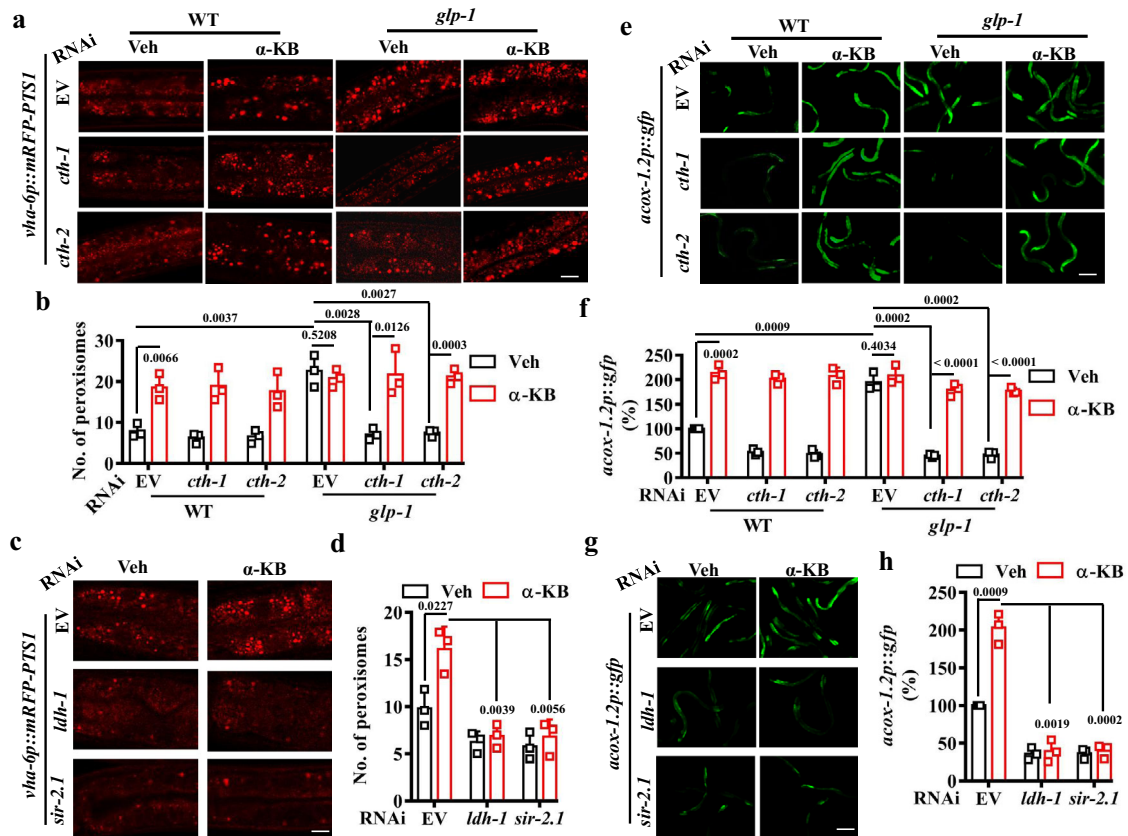


Fig. 3 | Alpha-KB promotes peroxisome function and biogenesis via the NAD⁺-SIR-2.1 pathway. a Representative images of peroxisomes in *glp-1(e2141ts)* mutant worms expressing *vha-6p::mRFP-PTS1*. Scale bars: 2.5 μ m. Veh vehicle. **b** The number of peroxisomes was increased in *glp-1(e2141ts)* mutants. RNAi knockdown of either *cth-1* or *cth-2* inhibited this increase, which was rescued by supplementation with α -ketobutyrate (α -KB, 500 μ M). Data were presented as mean values \pm SEM of three independent experiments ($n = 25$ worms per experiment). **c** Representative images of peroxisomes in transgenic worms expressing *vha-6p::mRFP-PTS1* after treatment with α -KB. **d** Supplementation with α -KB (500 μ M) increased the number of peroxisomes in worms, which was inhibited by RNAi knockdown of either *ldh-1* or *sir-2.1*. Data were presented as mean values \pm SEM of three independent experiments ($n = 25$ worms per experiment). **e** Representative

images of *acox-1.2p::gfp* in *glp-1(e2141ts)* worms. Scale bars: 150 μ m. **f** Expression of *acox-1.2p::gfp* was upregulated in *glp-1(e2141ts)* mutants. RNAi knockdown of either *cth-1* or *cth-2* inhibited this increase, which was rescued by supplementation with α -KB (500 μ M). Data were presented as mean values \pm SEM of three independent experiments ($n = 35$ worms per experiment). **g** Representative images of *acox-1.2p::gfp* in worms after treatment with α -KB. **h** Supplementation with α -KB (500 μ M) increased the expression of *acox-1.2p::gfp* in WT worms, which was inhibited by RNAi knockdown of either *ldh-1* or *sir-2.1*. Data were presented as mean values \pm SEM of three independent experiments ($n = 35$ worms per experiment). *P* values throughout were calculated using a one-way ANOVA followed by a Student–Newman–Keuls test. Source data are provided as a Source Data file.

Thus, peroxisome function is required for lifespan extension mediated by α -KB.

ROS are involved in life extension induced by germ-cell loss⁶. One of the products in the first step of peroxisomal fatty acid β -oxidation is H₂O₂, which is produced by acyl-CoA oxidases (ACOXs)⁴⁸. We thus asked whether H₂O₂ production was increased when peroxisome biogenesis is enhanced. Using a fluorescence dye DCHP⁴⁹, we found that the levels of H₂O₂ were increased in *glp-1(e2141ts)* mutants (Supplementary Fig. 14a, b). To determine which ACOX is involved in H₂O₂ formation, we screened the upregulated *acox* genes, including *acox-1.1*, *-1.2*, *-1.3*, *-1.4*, *-1.5*, *-1.6*, and *-3*, by RNAi. Of these seven genes, RNAi knockdown of *acox-1.2*, rather than the other six *acox* genes, significantly reduced the levels of H₂O₂ in *glp-1(e2141ts)* mutants (Supplementary Fig. 14c), suggesting that ACOX-1.2 is required for H₂O₂ production. Furthermore, supplementation with α -KB significantly promoted the production of H₂O₂ (Fig. 4c, d). We found that RNAi knockdown of *acox-1.2* not only inhibited H₂O₂ formation in WT worms, but also reduced the levels of H₂O₂ in WT α -KB-treated worms (Fig. 4c, d). Similar results were obtained by knockdown of *sir-2.1* by RNAi (Fig. 4c, d). These results suggest that H₂O₂ formation is induced by α -KB via ACOX-1.2.

To test whether the induction of H₂O₂ formation is involved in lifespan extension, an antioxidant N-acetylcysteine (NAC) was pre-treated with worms. H₂O₂ formation was markedly attenuated by NAC in α -KB-treated WT worms (Fig. 4c, d). Furthermore, supplementation with α -KB failed to extend the lifespan of either NAC- or *acox-1.2* RNAi-treated worms (Fig. 4e, f and Supplementary Data 1). Consistent with a previous observation¹⁵, NAC treatment shortened the lifespan of *glp-1(e2141ts)* mutants (Supplementary Fig. 15 and Supplementary Data 1). Although the knockdown of *acox-1.2* by RNAi also suppressed the lifespan of *glp-1(e2141ts)* mutants, it did not further reduce the lifespan of NAC-treated *glp-1(e2141ts)* mutants (Supplementary Fig. 15, Supplementary Data 1). Taken together, these results suggest that H₂O₂ production from peroxisomal fatty acid β -oxidation is crucial in α -KB-mediated lifespan extension.

SKN-1 is involved in α -KB-induced lifespan extension

How might H₂O₂ from peroxisomal fatty acid β -oxidation extend lifespan? The oxidative stress-response transcription factors DAF-16 and SKN-1, which are involved in lifespan extension in germline-defective worms^{20,50}, are potential candidates to serve as a downstream signal of H₂O₂. To test this hypothesis, we first determined whether α -KB activated SKN-1 and DAF-16. Utilizing transgenic worms expressing

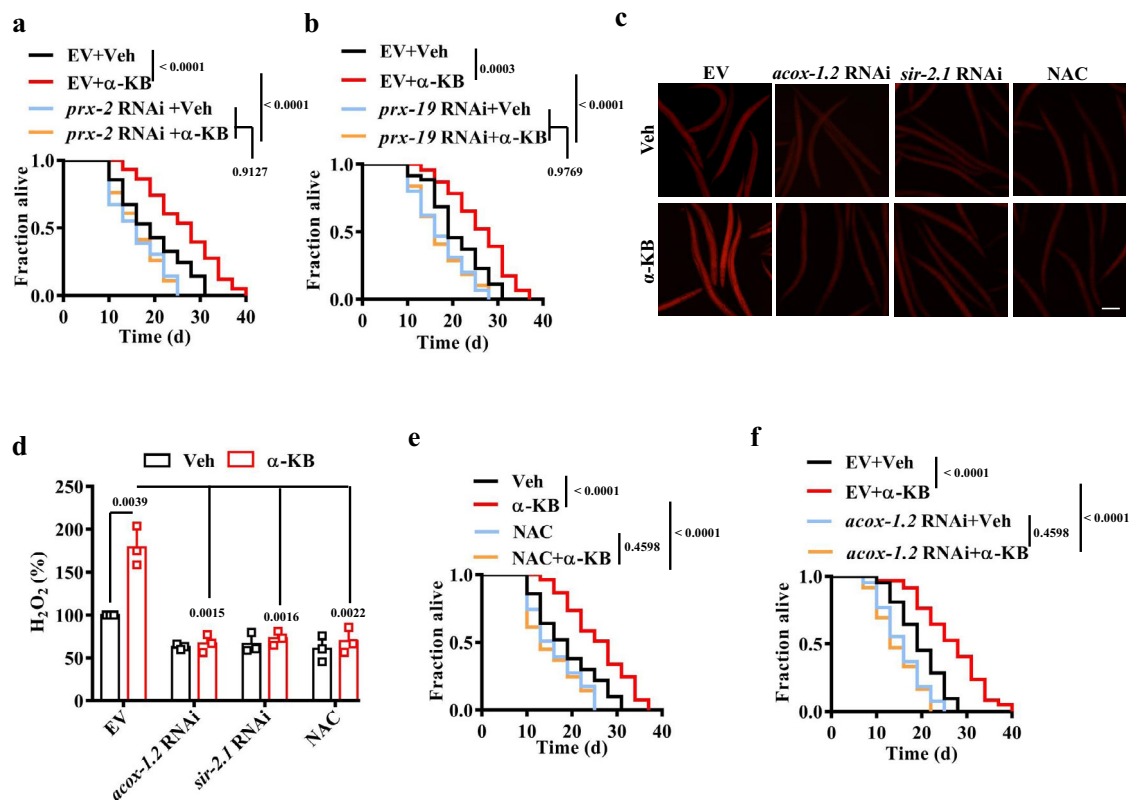


Fig. 4 | Peroxisome function and H₂O₂ production are involved in α-KB-mediated lifespan extension. **a, b** RNAi knockdown of *prx-2* (**a**) and *prx-19* (**b**) inhibited the lifespan extension of wild-type (WT) worms by treatment of α-ketobutyrate (α-KB, 500 μM). Veh vehicle. *P* values (**a, b**) were calculated using a log-rank test. **c** Representative images of H₂O₂ formation detected by fluorescence dye DCHP. Scale bars: 150 μm. **d** Quantification of fluorescence intensity. The levels of H₂O₂ were increased in WT worms treated with α-KB. RNAi knockdown of either *acox-1.2* or *sir-2.1* inhibited the levels of H₂O₂ in α-KB-treated WT worms. Data were

presented as mean values ± SEM of three independent experiments (*n* = 35 worms per experiment). *P* values were calculated using a one-way ANOVA followed by a Student–Newman–Keuls test. **e** Supplementation with N-acetylcysteine (NAC) (5 mM) shortened the lifespan of WT worms treated with α-KB (500 μM). **f** Knockdown of *acox-1.2* by RNAi suppressed the lifespan of WT worms treated with α-KB (500 μM). *P* values (**e, f**) were calculated using a log-rank test. See survival statistics in Supplementary Data 1. Source data are provided as a Source Data file.

skn-1p::skn-1::gfp and *daf-16p::daf-16::gfp*, we observed that α-KB supplementation promoted the nuclear translocation of SKN-1, but not DAF-16 (Fig. 5a, b and Supplementary Fig. 16a, b). Furthermore, the expression of *gst-4p::gfp*, a SKN-1 target gene, was upregulated by α-KB supplementation (Supplementary Fig. 17a, b). Next, NAC treatment inhibited the nuclear translocation of SKN-1 in WT worms treated with α-KB (Fig. 5a, b). Furthermore, the knockdown of *acox-1.2* by RNAi also significantly suppressed the nuclear translocation of SKN-1 in worms treated with α-KB (Fig. 5b). These results suggest that H₂O₂ from peroxisomal fatty acid β-oxidation activates SKN-1.

SKN-1 is needed for longevity in *glp-1(e214ts)* mutants²⁰. Likewise, the knockdown of *skn-1* by RNAi also inhibited the lifespan extension in WT worms supplemented with α-KB (Fig. 5c and Supplementary Data 1). As induction of autophagy is required for longevity in *glp-1(e214ts)* mutants^{51,52}, we hypothesized that the activation of SKN-1 by α-KB might promote autophagy in worms. We thus determined autophagy levels by using transgenic worms carrying GFP::LGG-1. During autophagic processes, LGG-1/ATG8 is sequestered at the membrane of autophagosomes and condenses into puncta, which is a reliable indicator of autophagy^{53,54}. The numbers of GFP::LGG-1-positive puncta in both the seam cells and the intestine in WT worms treated with α-KB were significantly higher than those in WT worms treated with vehicle (Fig. 5d, e). Knockdown of *skn-1* by RNAi substantially reduced the abundance of GFP::LGG-1 puncta in both the seam cells and the intestine in WT worms treated with α-KB (Fig. 5d, e).

The accumulation of LGG-1 puncta may result from either induction of autophagy or a block in autophagy at a late step. To distinguish between these possibilities, we monitored both autophagosomes and autolysosomes using transgenic worms expressing *lgg-1p::mCherry::GFP::lgg-1*. In these worms, autophagosomes are positive for both GFP and mCherry, whereas autolysosomes are only positive for mCherry as the low pH quenched GFP in autolysosomes⁵¹ (Supplementary Fig. 18a, b). We observed mCherry single-positive autolysosome puncta and mCherry/GFP double-positive autophagosome puncta in seam cells and the intestine of control worms. Supplementation with α-KB significantly increased the numbers of both autophagosome and autolysosome puncta in worms subjected to empty vector, but not *skn-1* RNAi. These results indicate that α-KB promotes autophagic flux via SKN-1.

Next, we asked whether SKN-1 modulates autophagy transcriptionally. Using qPCR, we determined the expressions of autophagy-related genes, including those involved in autophagosome formation and autophagic flux, such as *atg-2*, *atg-11*, *lgg-2*, *vps-34*, *sqst-1/SQSTM1/p62*, and *unc-51/ULK1/ATG1*; lysosome-autophagosome fusion, such as *lmp-1/LAMP-1* and *lmp-2/LAMP-1* genes with lysosomal functions, such as subunits of vacuolar ATPases (*vha-10* and *vha-14*), cathepsins (*Y16B4A.2*, *asp-3/cathepsin D*, *asp-4/cathepsin D*, and *tag-196/cathepsin F*), and *hlh-30/TFEB*. We found that most of these genes were upregulated in WT worms treated with α-KB (Supplementary Fig. 18c). Knockdown of *skn-1* by RNAi substantially reduced the

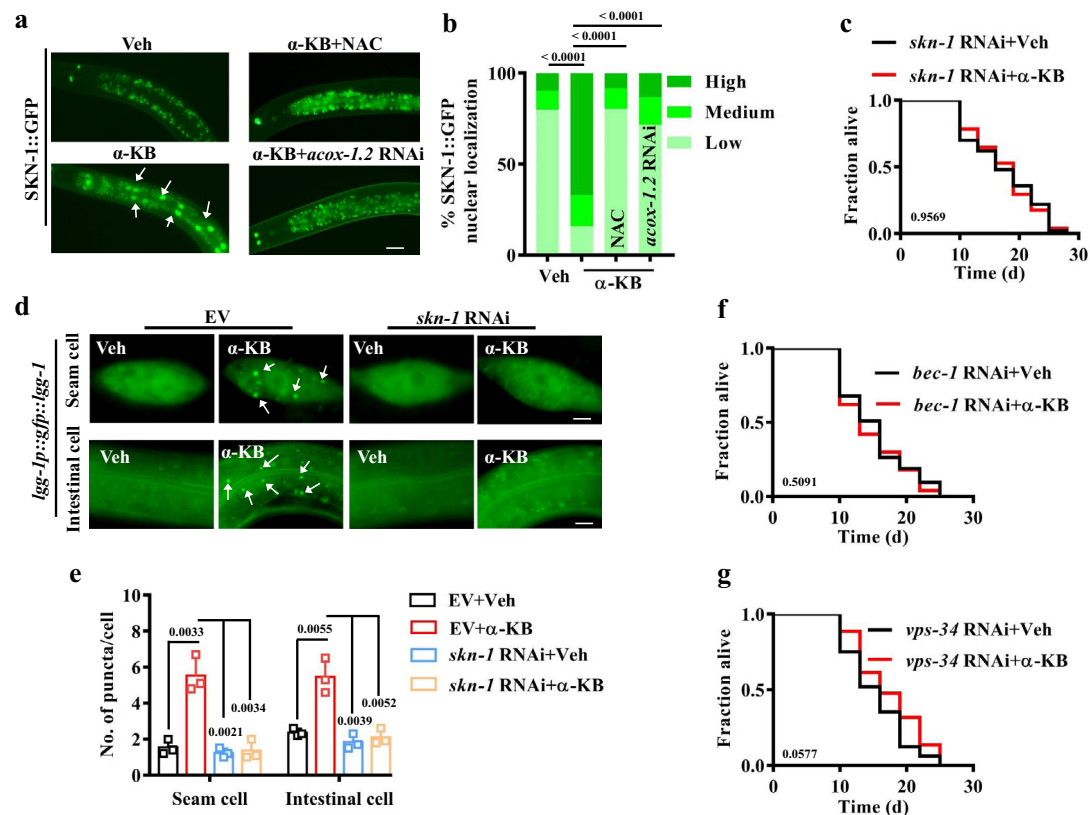


Fig. 5 | SKN-1-mediated autophagy is crucial for α -KB-induced lifespan extension. **a** Representative images of SKN-1::GFP translocation. Veh vehicle. Scale bars: 20 μ m. **b** Quantification of SKN-1 nuclear accumulation. Supplementation with α -ketobutyrate (α -KB, 500 μ M) promoted nuclear translocation of SKN-1::GFP in the intestine of worms, which was inhibited by treatment of *N*-acetylcysteine (NAC, 5 mM) or knockdown of *acox-1.2* by RNAi. Data were presented as mean values \pm SEM of three independent experiments ($n = 35$ worms per experiment). P values were calculated using the Friedman test (with Dunn's test for multiple comparisons). **c** Knockdown of *skn-1* by RNAi suppressed the lifespan of wild-type (WT) worms treated with α -KB (500 μ M). P value was calculated using a log-rank test.

d Representative images of autophagosomes (GFP::LGG-1 puncta) in the seam cells and intestinal cells of worms treated with α -KB (500 μ M). Scale bars: 5 μ m. **e** The numbers of GFP::LGG-1 puncta were counted. Data were presented as mean values \pm SEM of three independent experiments ($n = 35$ worms per experiment). P values were calculated using a one-way ANOVA followed by a Student–Newman–Keuls test. **f**, **g** Knockdown of either *bec-1* (**f**) or *vps-34* (**g**) by RNAi significantly reduced the lifespan of WT worms treated with α -KB (500 μ M). P values were calculated using a log-rank test. See survival statistics in Supplementary Data 1. Source data are provided as a Source Data file.

transcription of most of these genes. These data suggest that the change in the expression of these autophagy- and lysosome-related genes is transcriptionally regulated by SKN-1.

To test whether autophagy is required for SKN-1-mediated lifespan extension, two autophagy-related genes *bec-1* and *vps-34* were silenced by RNAi. Both BEC-1 (the *C. elegans* homolog of ATG6/VPS30/beclin1) and VPS-34 (the *C. elegans* homolog of the yeast phosphatidylinositol 3-kinase Vps34p) are key regulators of autophagy initiation and progression^{55,56}. We found that supplementation with α -KB failed to extend the lifespan of worms subjected to either *bec-1* or *vps-34* RNAi (Fig. 5f, g and Supplementary Data 1). These results indicate that SKN-1 is required for α -KB-induced lifespan extension by activating autophagy. As autophagy plays a crucial role in clearing damaged organelles, such as mitochondria, peroxisomes, and endoplasmic reticulum⁵⁷, these results also raised the possibility that the induction of autophagy by SKN-1, which is activated by H₂O₂ derived from the peroxisome, could, in turn, degrades the peroxisome itself. To test this hypothesis, we determined the number of peroxisomes in worms treated with α -KB with increasing incubation time. However, we found that the number of peroxisomes was elevated at 24, 36, and 48 h after the addition of α -KB (Supplementary Fig. 19a, b). Furthermore, RNAi knockdown of *skn-1* did not affect the increase in the number of peroxisomes in worms after the addition of α -KB.

Alpha-KB delays senescence in mammalian cells

Since supplementation with α -KB extends lifespan in worms, we next asked whether such an intervention is beneficial for controlling cellular aging. For this, we tested the effect of α -KB on cell senescence using senescent IMR90 cells at population doubling (PD) 50. We found that treatment with α -KB led to a significant increase in H₂O₂ formation (Fig. 6a, b). However, knockdown of either *SIRT1* or *ACO1* by RNAi or pre-treatment with NAC abrogated these effects of α -KB.

Next, we tested the effect of α -KB on nuclear location of NRF2, a feature that concurs with its activation⁵⁸. Immunofluorescence analysis with anti-total NRF2 antibodies revealed that NRF2 exhibited a dual nuclear and cytoplasmic distribution in IMR90 cells under basal conditions (Fig. 6c, d). Treatment of α -KB promoted NRF2 translocation to the nucleus, which was inhibited by si-*SIRT1*, si-*ACO1*, or NAC. We observed that phosphorylated NRF2 was exclusively located in the nucleus when detected using anti-phospho-NRF2(Ser40) antibodies (Supplementary Fig. 20a, b). Treatment of α -KB significantly increased the phosphorylated NRF2 levels in the nucleus, which was inhibited by si-*SIRT1*, si-*ACO1*, or NAC. These results suggest that α -KB activates NRF2 mediated by the SIRT1-ACO1 pathway.

Furthermore, we determined the effect of α -KB on autophagic activity by detecting LC3B-II levels. Upon the induction of autophagy, MAP1LC3B/LC3B (microtubule-associated protein 1 light chain 3b) is

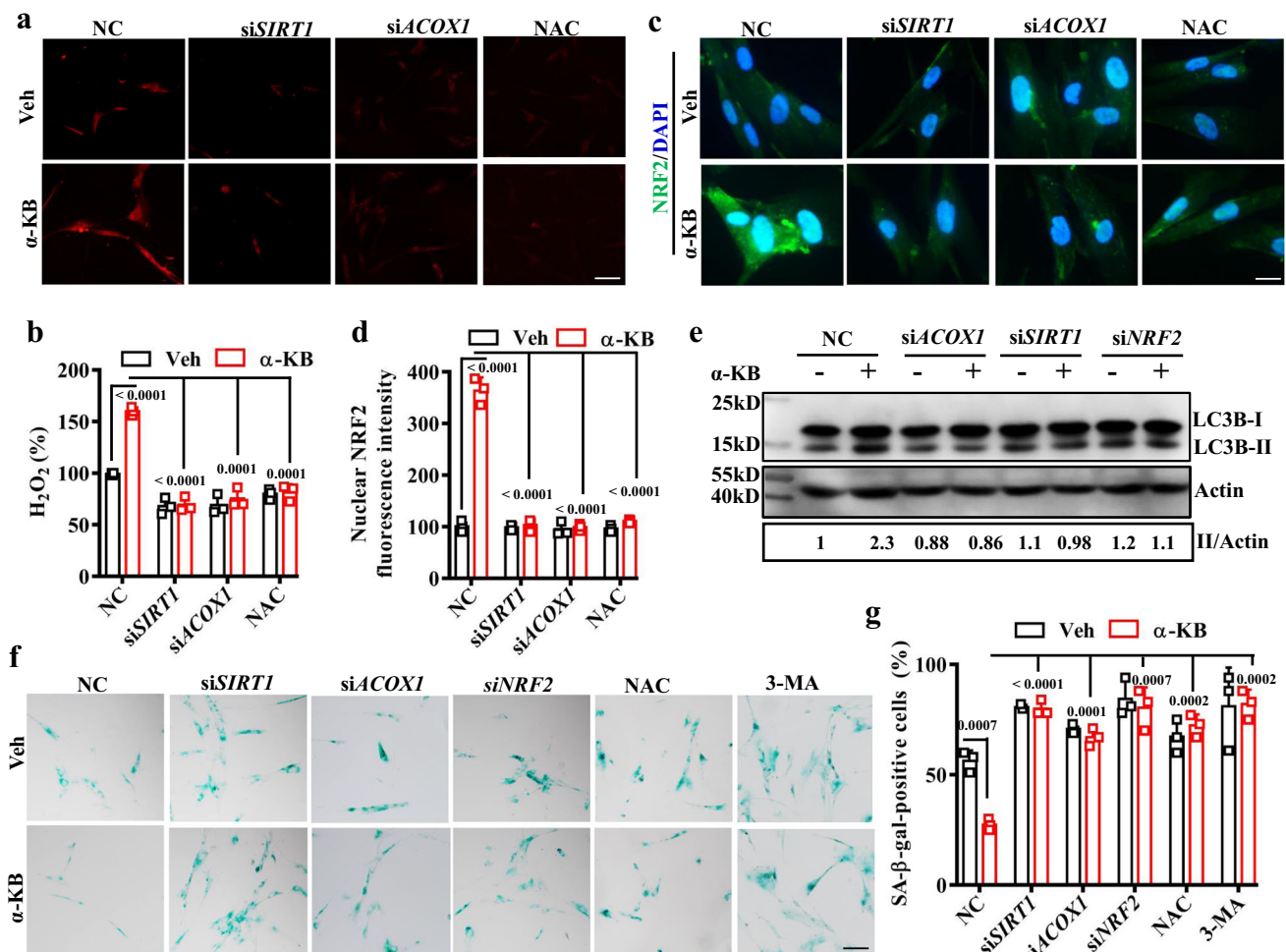


Fig. 6 | Alpha-KB delays senescence in mammalian cells. **a** Representative images of H₂O₂ formation detected by fluorescence dye DCHP in IMR90 cells. Scale bars: 15 μ m. **b** Quantification of Fluorescence intensity. The H₂O₂ levels were increased in cells treated with α -ketobutyrate (α -KB, 500 μ M) for 12 h, which was inhibited by RNAi knockdown of *SIRT1* or *ACO1*, or pre-treatment with *N*-acetylcysteine (NAC, 5 mM). Data were presented as mean values \pm SEM of three independent experiments. *P* values were calculated using a one-way ANOVA followed by a Student–Newman–Keuls test. **c** Representative images of immunofluorescence staining with anti-NRF2 antibodies. Scale bars: 5 μ m. **d** Quantification of fluorescence intensity of NRF2 in the nucleus. Supplementation with α -KB (500 μ M) induced nuclear accumulation of NRF2 in IMR90 cells, which was blocked by RNAi knockdown of *SIRT1* or *ACO1*, or pre-treatment with NAC (5 mM). Data were presented as mean values \pm SEM of three independent experiments. **e** Supplementation with α -KB (500 μ M) increased the protein levels of LC3B-II in worms, which was blocked by RNAi

knockdown of *SIRT1*, or *ACO1*, or pre-treatment with NAC (5 mM). The blot shown here is typical of three independent experiments. Data were presented as mean values \pm SEM of three independent experiments. *P* = 0.008, α -KB versus vehicle (veh); *P* = 0.0065, *ACO1* RNAi + α -KB versus α -KB; *P* = 0.0057, *SIRT1* RNAi + α -KB versus α -KB; *P* = 0.0112, *NRF2* RNAi + α -KB versus α -KB. **f** Representative images of senescence-associated β -galactosidase (SA- β -gal) staining. Scale bars: 15 μ m. **g** Quantification of SA- β -gal activity. Supplementation with α -KB (500 μ M) reduced the SA- β -gal activity. Knockdown of *SIRT1*, *ACO1*, or *NRF2* by RNAi, and pre-incubation of 3-MA (10 mM) abrogated the inhibitory effect of α -KB on SA- β -gal activity in cells treated with α -KB. Data were presented as mean values \pm SEM of three independent experiments. *P* values throughout were calculated using a one-way ANOVA followed by a Student–Newman–Keuls test. Veh vehicle, NC negative control. Source data are provided as a Source Data file.

cleaved at the carboxyl terminus and conjugated to phosphatidylethanolamine. The conversion of cytosolic LC3B (LC3B-I) to phagosome-associated LC3B-II is a marker for autophagy. We observed a dramatic increase in the protein levels of LC3B-II in IMR90 cells treated with α -KB (Fig. 6e). However, knockdown of *SIRT1*, *ACO1*, or *NRF2* by dsRNA significantly suppressed autophagy induced by α -KB. Finally, we determined the effect of α -KB on β -galactosidase activity, a well-established marker of cellular senescence⁵⁹. The addition of α -KB reduced the β -galactosidase activity (Fig. 6f, g). Pre-treatment of NAC or RNAi knockdown of *SIRT1*, *ACO1*, or *NRF2* significantly abrogated the inhibitory effect of α -KB on β -galactosidase (SA- β -gal) activity in IMR90 cells treated with α -KB. Likewise, pre-incubation of 3-methyladenine (3-MA) increased β -galactosidase activity and also abrogated the effect of α -KB (Fig. 6f, g). Together,

these results suggest that α -KB also provides beneficial effects in mammalian cells by inducing autophagy through the *SIRT1*-*ACO1*-H₂O₂-NRF2 pathway.

Discussion

Increased TSP activity promotes lifespan extension in both flies and worms^{4,5}. As an intermediate in TSP, H₂S functions to mediate longevity in yeast, worms, and fruit fly, and protect against hepatic ischemia-reperfusion injury^{1,4,6,15,60,61}. The central finding in this study is that supplementation with exogenous α -KB, another intermediate in TSP, extends *C. elegans* lifespan and delays senescence in fibroblast cells. This longevity effect is likely mediated by the augmentation of NAD⁺ via LDH-1. This increase in substrate allows for SIR-2.1/*SIRT1*-dependent increases in

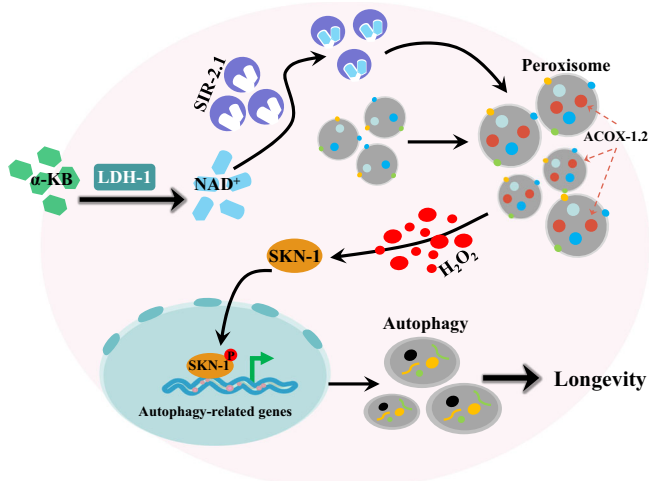


Fig. 7 | Schematic model for α -KB-mediated longevity. Supplementation with exogenous α -ketobutyrate (α -KB) increases the NAD^+ contents via LDH-1. The NAD^+ -SIRT-2.1/SIRT1 signaling enhances peroxisome function and biogenesis, thus leading to the upregulation of *acox-1.2/ACOX1*, a key gene in the peroxisomal fatty acid β -oxidation pathway. *ACOX-1.2/ACOX1* promotes the production of H_2O_2 , which in turn activates SKN-1/NRF2. This transcription factor induces autophagy by regulating the expressions of autophagic and lysosomal genes at a transcription level. Increased autophagic activity promotes longevity and delays cellular senescence.

peroxisome function and biogenesis, thus leading to upregulation of *acox-1.2/ACOX1*, a key gene in the peroxisomal fatty acid β -oxidation pathway. *ACOX-1.2/ACOX1* enhances the production of H_2O_2 , which subsequently activates SKN-1/NRF2. This transcription factor induces autophagy by driving the expression of autophagic and lysosomal genes, which in turn promotes longevity (Fig. 7). Our findings demonstrate a novel mechanism for extending lifespan that is mediated by an endogenous metabolite.

By mining two transcriptomic datasets^{20,28}, we show that there are ~50 peroxisomal genes upregulated in the long-lived germline-deficient worms. In contrast, a proteome analysis shows that the abundance of ~30 peroxisomal proteins is reduced, and protein import into the peroxisome is compromised in old worms³⁰. These omics data implicate an association between peroxisome and aging. However, until now, the exact role of peroxisome in aging and longevity remains largely unknown. While knockdown of peroxisomal genes *pex1/prx-1* and *pex13/prx-13* promotes lifespan in flies³², deletion of *pex5/prx-5* significantly shortens chronological lifespan in yeast³³. In long-lived double null *drp-1/fzo-1* mutant worms, the size of peroxisomes is significantly increased³¹. Inhibition of peroxisomal function by silencing *pex5/prx-5* almost blocks lifespan extension by a double mutation in *drp-1/fzo-1*. In this study, supplementation with α -KB remarkably increases the abundance and size of peroxisomes, which is required for lifespan extension by α -KB. Thus, our findings support the idea that enhanced peroxisome function may represent a common signature associated with longevity.

During aging, the intracellular NAD^+ levels are reduced in a variety of tissues in mammals^{62–64}. The increase in intracellular NAD^+ levels by supplementation of NAD^+ precursors such as NAM and NMN, or activation of the de novo NAD^+ synthesis pathway, improves lifespan and healthspan, and prevents age-associated metabolic dysfunction via a mechanism requiring SIRT1/SIR-2.1 in species ranging from mammals to worms^{9–11,41}. Our data show that the long-lived *glp-1(e214ts)* animals have higher NAD^+ levels, which are attributed to increased endogenous α -KB by CTH-1 and CTH-2. Furthermore, supplementation with exogenous α -KB increases the production of NAD^+ , thus extending the lifespan in WT worms in a SIRT1/SIR-2.1-dependent manner. These results suggest that α -KB exhibits its beneficial effect on delaying

senescence, at least in part, via the production of NAD^+ . The NAD^+ -SIRT1 pathway promotes longevity and prevents age-related physiological decline by inducing the mitochondrial unfolded protein response in worms and mammalian cells⁴¹. Moreover, NAD^+ augmentation significantly extends lifespan and improves healthspan by promoting mitophagy via SIRT1/SIRT2.1 in worm and mouse models of Ataxia Telangiectasia⁹, a rare autosomal recessive disease, and in worm and fly models of Werner syndrome⁶⁵, a human premature aging disease. In this study, our data demonstrate that supplementation with α -KB remarkably increases peroxisome function and biogenesis in WT worms in a SIRT2.1-dependent manner. Likewise, the NAD^+ precursors, including NAM, NMN, and NR, also induces an increase in peroxisome function and biogenesis in worms. Thus, our study identifies enhanced peroxisome function as a downstream mechanism underlying NAD^+ -SIRT-2.1-mediated longevity.

Although mitochondria are the main organelle responsible for ROS produced within cells, the peroxisome also generates ROS. In germline-deficient worms, the production of ROS is significantly elevated¹⁵. Besides these two sources of ROS (the mitochondrial ROS and DHE-reactive ROS produced by KRI-1)¹⁵, we show that H_2O_2 produced from the peroxisomal β -oxidation mediated by α -KB is another source of ROS in the germline-deficient worms. Accumulating evidence suggests that ROS may function as important modulators to promote lifespan in worms^{15,23–26,66,67}. Interestingly, younger cells or worms are capable of generating more ROS than older individuals in response to environmental stresses⁶⁸. Such redox-stress-response capacity is pivotal to maintain cellular redox and protein homeostasis. In the present study, α -KB-mediated H_2O_2 extends the lifespan in worms and delays cellular senescence by activating the ROS-sensitive transcription factor SKN-1/NRF2. SKN-1/NRF2 plays an important role in promoting longevity and delaying senescence in worms and mammals^{58,69,70}; however, it is not known whether SKN-1 exhibits its effect on longevity by modulating autophagy. We show that SKN-1 activates autophagy by initiating a transcriptional program that coordinates the different steps of the autophagic pathway, thereby extending the lifespan in worms. As NRF2 has been proven to positively modulate autophagy in mammalian cells⁷¹, it is concluded that, like HLH-30/TFEB⁵², SKN-1/NRF2 is probably another master regulator of autophagy across species.

In conclusion, our findings present new insights into the mechanism underlying endogenous metabolite-mediated longevity. Besides α -KB, other endogenous metabolites, such as oxaloacetate⁷², ω -6 polyunsaturated fatty acids⁷³, and α -ketoglutarate⁷⁴, can also delay aging and extend lifespan, suggesting that the key to longevity is hidden in our body. The endogenous metabolites provide new approaches for the prevention and treatment of aging and aging-related diseases.

Methods

Nematode strains

Multiple mutants and transgenic strains used in this study included *glp-1(e214ts)*, Strains BC14661 (sEx14661 [*rCes acox-1.2::GFP* + *pCeh361*]), CL2166 (*dvIs19* [(*pAF15*)*gst-4p::GFP::NLS*]), *eat-2(ad1116)*, *daf-2(e1370)*, *isp-1(qm150)*, and AM140 (*rmls132[unc-54p::Q35::YFP]*) were kindly provided by the Caenorhabditis Genetics Center (CGC; <http://www.cbs.umn.edu/CGC>), funded by NIH Office of Research Infrastructure Programs (P40 OD010440). The nematode strains VS10 (*hJIs37* [*vha-6p::mRFP-PTS1* + *Cbr-unc-119(+)*]), DA2123 (*adIs2122* [*lgg-1p::GFP::lgg-1* + *rol-6(su1006)*]), (*hqls181[sdhl-1p::mtLs::gfp]*), MAH215 (*sqIs11[lgg-1p::mCherry::GFP::lgg-1]*), *pmp-2p::pmp-2::mCherry*, and *prx-11p::prx-11::gfp* were kindly provided by Drs. Bin Liang (Yunnan University), Bin Qi (Yunnan University), Meng-Qiu Dong (National Institute of Biological Sciences, Beijing), Hong Zhang (Institute of Biophysics, Chinese Academy of Science), and Huanhu Zhu (ShanghaiTech University), respectively. Mutants were backcrossed three times into the

N2 strain used in the laboratory. All strains were grown on nematode growth media (NGM) plates with *E. coli* OP50 at 20 °C⁷⁵.

Cell culture

The human lung fibroblast IMR90 cells were a gift from Dr. Xudong Zhao (Sichuan University West China Medical School) and obtained from the American Type Culture Collection (ATCC; CCL-186). The cells were grown in MEM with 1% sodium pyruvate, 1% penicillin-streptomycin, and 10% fetal bovine serum (Gibco, A3161001C) in a humidified, 5% CO₂:95% air incubator at 37 °C. When attained 50 PD, IMR90 cells were treated with 500 μM of α-KB (MACKLIN, C10962521), 5 mM NAC (MACKLIN, N800425), or 10 mM 3-Methyladenine (MACKLIN, 5142-23-4). ddH₂O or DMSO was used as a control.

RNA interference for worms

RNAi bacterial strains containing targeting genes were obtained from the Ahringer RNAi library⁷⁶. Briefly, *E. coli* strain HT115(DE3) expressing dsRNA corresponding to each worm gene was grown overnight in LB broth containing 100 μg/ml ampicillin at 37 °C, then spread onto NGM plates containing 100 μg/ml ampicillin and 5 mM isopropyl 1-thio-β-D-galactopyranoside (IPTG). The RNAi-expressing bacteria were then grown overnight at 25 °C. Synchronized L1 larvae were placed on the seeded RNAi plates at 20 °C until animals reached maturity. Young adult worms were used for further experiments.

RNA interference for cells

All chemically synthesized siRNAs were obtained from Gene-Pharma Corporation. To silence the expression of *SIRT1*, *ACO1*, or *NRF2* by RNAi, IMR90 cells were transfected at 50% confluence with 100 nM of siRNAs in Opti-MEM medium using Lipofectamine 2000 transfection agent (Thermo Fisher, 11668019). Gene silencing efficiency was confirmed by quantitative real-time PCR 72 h post-transfection. The following siRNAs were used (sequence of the sense strand): *SIRT1*, 5'-GGGAAAUGUAUUGGCAGUGUU-3' (F), 5'-CACUGCCAAUACAUUUCC CUU-3' (R); *ACO1*, 5'-UCAUCUAAGAGACCUAGGCTT-3' (F), 5'-GCCUA GGUCUCUUAGAUGATT-3' (R); *NRF2*, 5'-UCAUCUAAGAGACCUAGG CTT-3' (F), 5'-GCCUAGGUCUCUUAGAUGATT-3' (R); negative control 5'-UUCUCCGAACGUGUCACGUTT-3' (F), 5'-ACGUGACACGUUCGGAG AATT-3' (R).

DAVID enrichment analysis

We annotated two published transcriptomic datasets (GSE43864 and GSE63075)^{20,28} based on the Wormbase database, of version WS236 (www.wormbase.org). We searched for enrichment of KEGG (Kyoto Encyclopedia of Genes and Genomes) pathway gene sets and GO terms using the 3208 upregulated genes overlapped between these two transcriptomic datasets. Identify enriched GO terms and KEGG pathway of the overlapped genes of the expression profiles from these two datasets by Database for Annotation, Visualization, and Integrated Discovery (DAVID) version 6.7 (<https://david.ncifcrf.gov/home.jsp>)⁷⁷. GO term or KEGG pathway with an adjusted *p* value <0.01 was defined as significantly changed.

Drug treatment

NGM agar plates seeded with *E. coli* OP50 were supplemented with 200 and 500 μM of α-KB, or 200 and 500 μM of NAM (MERCK, 98-92-0), or 200 and 500 μM of NMN (MedChemExpress (MCE), HY-F0004), or 200 and 500 μM of NR (MedChemExpress(MCE), HY-123033A), or 5 mM NAC. ddH₂O or DMSO was used as a control.

Lifespan analysis

Synchronized populations of young adult worms were grown on NGM agar plates seeded with *E. coli* OP50 and tested drugs at 20 °C to score lifespan³⁷. To test the effect of drugs on lifespan,

the *E. coli* OP50-seeded NGM agar plates were supplemented with these drugs. The first day of adulthood of animals was recorded as day 1. Worms were transferred to new plates every day during their reproductive period. After reproduction ceases, worms were transferred every three days. The number of worms was counted every day. Worms that did not move when gently prodded and lacking pharyngeal pumping were marked as dead. Three plates of 50–60 worms per plate were tested per assay and all experiments were performed three times independently. Life spans for each assay are provided in Supplementary Data 1.

Age-related phenotypic marker assays in worms

On the first day of adulthood, animals were placed on NGM agar plates containing *E. coli* OP50 until day 8 of adulthood and the following age-related phenotypes were scored. (1) Pharyngeal pumping was determined by counting the number of contractions in the terminal bulb of the pharynx in 30-s intervals. (2) Body bending was measured by counting the number of body bends in 30 s intervals. 20–30 worms were examined per assay in three independent experiments.

Detection of H₂S in worms

The endogenous H₂S levels in germline-deficient animals were determined using a lysosome-targeted fluorescent chemodosimeter according to the previously described method³⁴. Briefly, worms were incubated in Petri dishes filled with M9 buffer containing the fluorescent chemodosimeter (10 μM) at 20 °C for 3 h. The worms then were washed three times with M9 buffer and mounted in M9 onto microscope slides. The slides were viewed using a Zeiss Axioskop 2 Plus fluorescence microscope. The brighter the blue coloration, the stronger the fluorescence signal intensity. At least 30 worms were examined per assay in three independent experiments.

Measurement of α-KB by LC/MS

The levels of α-KB in adult worms were determined by LC/MS. Briefly, after ~5 ml of packed worms were (Scanvac-Collsafe 110-4, LaboGene, Lynge, Denmark) for 48 h. The worm samples were then mixed with 2 ml of lysis buffer RIPA (Beyotime Institute of Biotechnology, Haimen, China), and gently ultrasonicated for 20 min. The mixture was centrifuged at 16,600×g for 30 min at 4 °C, and the supernatant was collected and then extracted with ethyl acetate. After the final centrifugation, the supernatant was collected, and analyzed by the Thermo Scientific Dionex Ultimate 3000 UHPLC system equipped with a Thermo high-resolution Q Exactive focus mass spectrometer (Thermo, Bremen, Germany). Samples were separated on a ZORBAX SB-C18 (4.6 mm × 250 mm, 5 μm particles; Agilent Technologies) with gradient elution. Ten microliters of samples were injected into the column using an autosampler. The mobile phase consisted of solvent A (water) containing 0.1% formic acid and solvent B (methanol), The flow rate of the mobile phase was 1 ml/min. The gradient program was as follows: 0–2 min (5% B), 2–8 min (5–15% B), 8–12 min (15–98% B), 12–16 min (98% B), 16–20 min (5% B). The instrument settings were as follows: capillary temperature of 320 °C, sheath gas flow rate of 35 (arbitrary units), an auxiliary gas flow rate of 15 (arb), spray voltage of ~2.5 kV, full MS resolution of 70,000. Data were analyzed by using Thermo Scientific Xcaliber 4.4 software.

Intestinal barrier function assay in worms

Intestinal barrier function was determined according to the method described previously⁷⁸. Briefly, young adult worms were grown on standard NGM plates in the presence or absence of α-KB (500 μM) at 20 °C for 10 days. After being removed from the NGM plates, these worms were suspended in an M9 liquid medium containing *E. coli* OP50 (OD = ~0.6), 5% food dye FD&C Blue No. 1 (Bis[4-(*N*-ethyl-*N*-3-sulfophenylmethyl) aminophenyl]-2-sulfophenylmethyl disodium salt) (AccuStandard, New Haven, CT),

and further incubated for 6 h. After washing with M9 buffer four times, the worms were mounted in M9 onto microscope slides. The slides were viewed using a Zeiss Axioskop 2 Plus fluorescence microscope (Carl Zeiss, Jena, Germany) to measure the leakage of the dyes in the body cavity. The rate of body-cavity leakage was calculated as a percentage by dividing the number of worms with dye leakage by the number of total worms. Five independent experiments were carried out. In each experiment, at least 20 of worms were calculated.

NAD⁺ measurements by LC/MS

NAD⁺ in worms was extracted by the method described previously¹¹. Briefly, after ~1 ml of packed worms were freeze-dried in a freeze dryer (Scanvac-Collsafe 110-4, LaboGene, Lyngø, Denmark) for 24 h. The worm samples then were extracted with 10% perchloric acid and neutralized in 3 M K₂CO₃ on ice. After centrifuged at 16,600 × g for 30 min at 4 °C to remove the insoluble residue, the supernatant was filtered, and analyzed by Thermo Scientific Dionex Ultimate 3000 UHPLC system equipped with a Thermo high-resolution Q Exactive focus mass spectrometer (Thermo, Bremen, Germany). Samples were separated on a ZORBAX SB-C18 (4.6 mm × 250 mm, 5 μm particles; Agilent Technologies) with gradient elution. Ten microliters of samples were injected into the column using an autosampler. The mobile phase consisted of solvent A (water) containing 0.1% formic acid and solvent B (methanol). The flow rate of the mobile phase was 1 ml/min. The method to measure NAD⁺ content is as follows: The gradient program was as follows: 0–2 min (2% B), 2–8 min (2–15% B), and 8–12 min (15–98% B), 12–16 min (98% B), 16–20 min (2% B). The instrument settings were as follows: capillary temperature of 350 °C, sheath gas flow rate of 35 (arbitrary units), an auxiliary gas flow rate of 15 (arb), spray voltage of 3.5 kV, full MS resolution of 70,000. The column temperature was set to 40 °C. Data were analyzed by using Thermo Scientific Xcaliber 4.4 software.

Detection of H₂O₂ in worms

The H₂O₂ levels in worms were determined using a fluorescence dye, DCHP, according to the previously described method⁴⁹. Briefly, worms were incubated in Petri dishes filled with M9 buffer containing DCHP (10 μM) at 20 °C for 5 h. Then, worms were washed with M9 buffer three times and mounted in M9 onto microscope slides. The slides were viewed using a Zeiss Axioskop 2 Plus fluorescence microscope. At least 30 worms were examined per assay in three independent experiments.

Quantitative RT-PCR

Total RNA was extracted from worms with TRIzol Reagent (Invitrogen, Carlsbad, CA). Random-primed cDNAs were generated by reverse transcription of the total RNA samples with SuperScript II (Invitrogen). Quantitative real-time PCR analysis was performed using SYBR Premix (Takara, Dalian, China) on a Roche LightCycler 480 System (Roche Applied Science, Penzberg, Germany). The relative amount of each mRNA to *act-1* mRNA (an internal control) was calculated using the method described previously⁷⁹. The primers used for qPCR assays are listed in Supplementary Data 2, respectively.

Western blotting

Worms or cells were collected and lysed on ice for 30 min in lysis buffer RIPA (Beyotime Institute of Biotechnology, Haimen, China). The supernatant was obtained from cell lysates by centrifugation at 16,600 × g for 20 min at 4 °C and used for Western blot analysis. The proteins of lysates (50 μg per well) were separated on a 10% sodium dodecyl sulfate-polyacrylamide gel and then transferred to polyvinylidene fluoride membranes. The primary antibodies were anti-LC3B mAb (#3868, 1:3000 dilution, Cell Signaling Technology, Danvers, MA), anti-Phospho-AMPKα(Thr172) mAb (#2535, 1:1000 dilution,

Cell Signaling Technology), anti-β-Actin mAb (#sc-8432, 1:4000 dilution, Santa Cruz Biotechnology, Santa Cruz, CA), and anti-AMPKα antibodies (#2532 S, 1:1000 dilution, Cell Signaling Technology). The secondary antibodies used were HRP-conjugated anti-mouse (#7074 s, 1:3000 dilution, Cell Signaling Technology) or anti-rabbit IgG (#7076p2, 1:3000 dilution, Cell Signaling Technology). An imaging system (Amersham Imager 600) was used for the documentation of the Western blot results.

The quantification of peroxisome numbers and size

To determine the function and biogenesis of peroxisomes, we used the transgenic worms expressing *vha-6p::mRFP-PTS1*³¹, *pmp-2p::pmp-2::mCherry*, and *prx-11p::prx-11::gfp*⁴⁶. Briefly, worms were collected and transferred in an Eppendorf tube filled with M9 buffer containing 4% formaldehyde at 20 °C for 5 min. After washing with M9 buffer three times, the worms were mounted in M9 onto microscope slides. The mRFP-PTS1, PMP-2::mCherry, and PRX-11::GFP fluorescence signals were acquired by Leica TCS SP8 STED confocal microscope (Leica Microsystems, Wetzlar, Germany) at 63x magnification. Confocal images were taken from the Int1 and Int2 cells (the first two anterior ring of the intestine). The diameters of peroxisomes were 0.1–1.2 μm⁸⁰, as a standard for quantifying the number and size of peroxisomes. At least 20 worms were examined per assay in three independent experiments.

Scoring of SKN-1 and DAF-16 nuclear accumulation

Young adult worms expressing *skn-1p::skn-1::gfp* or *daf-16p::daf-16::gfp* were grown on NGM agar plates containing *E. coli* OP50. After being treated with 500 μM α-KB for 24 h, the worms were immediately mounted in M9 onto microscope slides. The slides were viewed using a Zeiss Axioskop 2 Plus fluorescence microscope. The status of DAF-16::GFP localization was categorized as cytosolic localization or nuclear localization when localization was observed throughout the body from head to tail⁸¹. When nuclear localization was visible, but not completely throughout the body, the status of DAF-16::GFP localization was characterized as intermediate localization. At least 30 worms were examined per assay in three independent experiments. SKN-1::GFP accumulation in intestinal nuclei was scored as previously described⁸². “High” indicates that a strong SKN-1::GFP signal was present in all nuclei, “medium” indicates that nuclear SKN-1::GFP was detected in both anterior and posterior intestinal nuclei, and “low” indicates that nuclear SKN-1::GFP was barely detectable in either anterior or posterior intestinal nuclei.

Autophagy analysis

Young adult worms expressing GFP::LGG-1 were grown on NGM agar plates containing *E. coli* OP50 in the presence or absence of 500 μM α-KB. After 24 h of growth, the worms were immediately mounted in M9 onto microscope slides. The slides were viewed using a Zeiss Axioskop 2 Plus fluorescence microscope. GFP::LGG-1 positive puncta were counted in the seam cells or the intestine. At least 30 worms were examined per assay in three independent experiments.

Microscopy

The transgenic worms carrying *acox-1.2p::gfp* or *gst-4p::gfp* were treated with 500 μM α-KB for 12 and 24 h. The worms were mounted in M9 onto microscope slides for detecting fluorescent signals. The slides were viewed using a Zeiss Axioskop 2 Plus fluorescence microscope. At least 30 worms were examined per assay in three independent experiments. The fluorescence intensity was analyzed using ImageJ² × V2.1.4.8 (NIH).

Immunofluorescence

Cells were fixed with 4% paraformaldehyde (PFA) for 10 min at room temperature. After washed with PBS three times and were treated with

PBS containing 0.1% Triton X-100 for 15 min, the cells were permeabilized, and blocked with PBST containing 5% fetal bovine serum for 90 min at room temperature. Then the cells were immunostained with anti-NRF2 mAb (#2F6C6, 1:500 dilution, Cusabio Technology LLC, Houston, TX) or anti-Phospho-NRF2(Ser40) antibodies (PA5-67520, 1:500 dilution, Thermo Fisher Scientific) overnight at 4 °C. After washed three times with 0.1% Tween-20 in PBS (PBST), these cells were incubated with Alexa Fluor 405 anti-mouse IgG (H + L) (A-55057, 1:200 dilution, Thermo Fisher Scientific) or Alexa Fluor 488 anti-Rabbit IgG (H + L) (A-21206, 1:200 dilution, Thermo Fisher Scientific) for 1 h. Then, the slides were washed three times with PBST and stained with 1 µg/ml of 4,6-diamidino-2-phenylindole (DAPI) for 30 min to detect nuclei. Images were acquired using a Zeiss Axioskop 2 plus fluorescence microscope (Carl Zeiss, Jena, Germany).

Senescence-associated β -galactosidase staining

Senescence-associated SA- β -gal staining was performed according to the method described previously⁸³. Briefly, IMR90 cells were fixed in 2% formaldehyde and 0.2% glutaraldehyde at room temperature for 10 min, and stained in freshly prepared staining solution (all reagents were from Cell Senescence β -galactosidase Staining Kit, Beyotime, Haimen) at 37 °C overnight. Images were taken and the percentages of SA- β -gal-positive cells were counted and determined using Image J. Each group had three biological replicates.

Statistical analysis

All statistical tests were two-sided, and values of $P < 0.05$ were considered statistically significant. Differences in survival rates were analyzed using the log-rank test. Differences in gene expression, mRNA and protein levels, the contents of metabolites and H₂O₂, the percentages of SA- β -gal-positive cells, the numbers of GFP::LGG-1 positive puncta, and fluorescence intensity were assessed by performing one-way ANOVA followed by the Student–Newman–Keuls test or the Student's t -test. Differences in the distribution of SKN-1 were analyzed using the Friedman test (with Dunn's test for multiple comparisons) or the Wilcoxon signed-rank test. To test for significant overlap between different gene lists, Fisher's exact test was used. Data were analyzed using GraphPad Prism 7 (GraphPad Software Inc., La Jolla, CA).

Reporting summary

Further information on research design is available in the Nature Portfolio Reporting Summary linked to this article.

Data availability

The data supporting the findings of this study are available within the article and its supplementary materials. Lifespan data were collected in Supplementary Data 1. The primers used for qRT-PCR are listed in Supplementary Data 2. The transcriptome data that support the findings of this study are available in a publicly accessible repository from the GEO under accession [GSE43864](https://www.ncbi.nlm.nih.gov/geo/query/acc.cgi?acc=GSE43864) and [GSE63075](https://www.ncbi.nlm.nih.gov/geo/query/acc.cgi?acc=GSE63075). Source data are provided with this paper.

References

- Hine, C. & Mitchell, J. R. Calorie restriction and methionine restriction in control of endogenous hydrogen sulfide production by the transsulfuration pathway. *Exp. Gerontol.* **68**, 26–32 (2015).
- Hine, C., Zhu, Y., Hollenberg, A. N. & Mitchell, J. R. Dietary and endocrine regulation of endogenous hydrogen sulfide production: implications for longevity. *Antioxid. Redox Signal.* **28**, 1483–1502 (2018).
- Kabil, O., Vitvitsky, V., Xie, P. & Banerjee, R. The quantitative significance of the transsulfuration enzymes for H₂S production in murine tissues. *Antioxid. Redox Signal.* **15**, 363–372 (2011).
- Hine, C. et al. Endogenous hydrogen sulfide production is essential for dietary restriction benefits. *Cell* **160**, 132–144 (2015).
- Kabil, H., Kabil, O., Banerjee, R., Harshman, L. G. & Pletcher, S. D. Increased transsulfuration mediates longevity and dietary restriction in *Drosophila*. *Proc. Natl Acad. Sci. USA* **108**, 16831–16836 (2011).
- Miller, D. L. & Roth, M. B. Hydrogen sulfide increases thermotolerance and lifespan in *Caenorhabditis elegans*. *Proc. Natl Acad. Sci. USA* **104**, 20618–20622 (2007).
- Qabazard, B. et al. Hydrogen sulfide is an endogenous regulator of aging in *Caenorhabditis elegans*. *Antioxid. Redox Signal.* **20**, 2621–2630 (2014).
- Das, A. et al. Impairment of an endothelial NAD(+)-H₂S signaling network is a reversible cause of vascular aging. *Cell* **173**, 74–89.e20 (2018).
- Fang, E. F. et al. NAD(+) replenishment improves lifespan and healthspan in ataxia telangiectasia models via mitophagy and DNA repair. *Cell Metab.* **24**, 566–581 (2016).
- Hashimoto, T., Horikawa, M., Nomura, T. & Sakamoto, K. Nicotinamide adenine dinucleotide extends the lifespan of *Caenorhabditis elegans* mediated by sir-2.1 and daf-16. *Biogerontology* **11**, 31–43 (2010).
- Katsyuba, E. et al. De novo NAD(+) synthesis enhances mitochondrial function and improves health. *Nature* **563**, 354–359 (2018).
- Mouchiroud, L. et al. The NAD+/sirtuin pathway modulates longevity through activation of mitochondrial UPR and FOXO signaling. *Cell* **154**, 430–441 (2013).
- Kimble, J. & Crittenden, S. L. Controls of germline stem cells, entry into meiosis, and the sperm/oocyte decision in *Caenorhabditis elegans*. *Annu. Rev. Cell Dev. Biol.* **23**, 405–433 (2007).
- Arantes-Oliveira, N., Apfeld, J., Dillin, A. & Kenyon, C. Regulation of life-span by germ-line stem cells in *Caenorhabditis elegans*. *Science* **295**, 502–505 (2002).
- Wei, Y. & Kenyon, C. Roles for ROS and hydrogen sulfide in the longevity response to germline loss in *Caenorhabditis elegans*. *Proc. Natl Acad. Sci. USA* **113**, E2832–E2841 (2016).
- Goudeau, J. et al. Fatty acid desaturation links germ cell loss to longevity through NHR-80/HNF4 in *C. elegans*. *PLoS Biol.* **9**, e1000599 (2011).
- Hsin, H. & Kenyon, C. Signals from the reproductive system regulate the lifespan of *C. elegans*. *Nature* **399**, 362–366 (1999).
- Lapierre, L. R., Gelino, S., Meléndez, A. & Hansen, M. Autophagy and lipid metabolism coordinately modulate life span in germline-less *C. elegans*. *Curr. Biol.* **21**, 1507–1514 (2011).
- Shen, Y., Wollam, J., Magner, D., Karalay, O. & Antebi, A. A steroid receptor-microRNA switch regulates life span in response to signals from the gonad. *Science* **338**, 1472–1476 (2012).
- Steinbaugh, M. J. et al. Lipid-mediated regulation of SKN-1/Nrf in response to germ cell absence. *Elife* **4**, e07836 (2015).
- Yamawaki, T. M. et al. The somatic reproductive tissues of *C. elegans* promote longevity through steroid hormone signaling. *PLoS Biol.* **8**, e1000468 (2010).
- Wang, M. C., O'Rourke, E. J. & Ruvkun, G. Fat metabolism links germline stem cells and longevity in *C. elegans*. *Science* **322**, 957–960 (2008).
- Lee, S. J., Hwang, A. B. & Kenyon, C. Inhibition of respiration extends *C. elegans* life span via reactive oxygen species that increase HIF-1 activity. *Curr. Biol.* **20**, 2131–2136 (2010).
- Yang, W. & Hekimi, S. A mitochondrial superoxide signal triggers increased longevity in *Caenorhabditis elegans*. *PLoS Biol.* **8**, e1000556 (2010).
- Schulz, T. J. et al. Glucose restriction extends *Caenorhabditis elegans* life span by inducing mitochondrial respiration and increasing oxidative stress. *Cell Metab.* **6**, 280–293 (2007).

26. Yee, C., Yang, W. & Hekimi, S. The intrinsic apoptosis pathway mediates the pro-longevity response to mitochondrial ROS in *C. elegans*. *Cell* **157**, 897–909 (2014).
27. Hwang, A. B. et al. Feedback regulation via AMPK and HIF-1 mediates ROS-dependent longevity in *Caenorhabditis elegans*. *Proc. Natl Acad. Sci. USA* **111**, E4458–E4467 (2014).
28. Gracida, X. & Eckmann, C. R. Fertility and germline stem cell maintenance under different diets requires *nhr-114/HNF4* in *C. elegans*. *Curr. Biol.* **23**, 607–613 (2013).
29. Lodhi, I. J. & Semenkovich, C. F. Peroxisomes: a nexus for lipid metabolism and cellular signaling. *Cell Metab.* **19**, 380–392 (2014).
30. Narayan, V. et al. Deep proteome analysis identifies age-related processes in *C. elegans*. *Cell Syst.* **3**, 144–159 (2016).
31. Weir, H. J. et al. Dietary restriction and AMPK increase lifespan via mitochondrial network and peroxisome remodeling. *Cell Metab.* **26**, 884–896.e885 (2017).
32. Zhou, B. et al. Midlife gene expressions identify modulators of aging through dietary interventions. *Proc. Natl Acad. Sci. USA* **109**, E1201–E1209 (2012).
33. Lefevre, S. D., van Roermund, C. W., Wanders, R. J., Veenhuis, M. & van der Klei, I. J. The significance of peroxisome function in chronological aging of *Saccharomyces cerevisiae*. *Aging cell* **12**, 784–793 (2013).
34. Zou, X. J. et al. A lysosome-targeted fluorescent chemodosimeter for monitoring endogenous and exogenous hydrogen sulfide by in vivo imaging. *Chem. Commun.* **50**, 13833–13836 (2014).
35. Qabazard, B. et al. Hydrogen sulfide is an endogenous regulator of aging in *Caenorhabditis elegans*. *Antioxid. Redox Signal.* **20**, 2621–2630 (2014).
36. Zivanovic, J. et al. Selective persulfide detection reveals evolutionarily conserved antiaging effects of S-sulfhydration. *Cell Metab.* **30**, 1152–1170.e1113 (2019).
37. Chen, Y. L. et al. Adiponectin receptor PAQR-2 signaling senses low temperature to promote *C. elegans* longevity by regulating autophagy. *Nat. Commun.* **10**, 2602 (2019).
38. Garigan, D. et al. Genetic analysis of tissue aging in *Caenorhabditis elegans*: a role for heat-shock factor and bacterial proliferation. *Genetics* **161**, 1101–1112 (2002).
39. Roux, A. E., Langhans, K., Huynh, W. & Kenyon, C. Reversible age-related phenotypes induced during larval quiescence in *C. elegans*. *Cell Metab.* **23**, 1113–1126 (2016).
40. Lin, S. J., Defossez, P. A. & Guarente, L. Requirement of NAD and SIR2 for life-span extension by calorie restriction in *Saccharomyces cerevisiae*. *Science* **289**, 2126–2128 (2000).
41. Mouchiroud, L. et al. The NAD(+)/sirtuin pathway modulates longevity through activation of mitochondrial UPR and FOXO signaling. *Cell* **154**, 430–441 (2013).
42. Schmeisser, K. et al. Role of sirtuins in lifespan regulation is linked to methylation of nicotinamide. *Nat. Chem. Biol.* **9**, 693–700 (2013).
43. von Morze, C. et al. Hyperpolarized [(13)C]ketobutyrate, a molecular analog of pyruvate with modified specificity for LDH isoforms. *Magn. Reson. Med.* **75**, 1894–1900 (2016).
44. Sullivan, L. B. et al. Supporting aspartate biosynthesis is an essential function of respiration in proliferating cells. *Cell* **162**, 552–563 (2015).
45. Thieringer, H., Moellers, B., Dodt, G., Kunau, W. H. & Driscoll, M. Modeling human peroxisome biogenesis disorders in the nematode *Caenorhabditis elegans*. *J. Cell Sci.* **116**, 1797–1804 (2003).
46. Li, N. et al. A sphingolipid-mTORC1 nutrient-sensing pathway regulates animal development by an intestinal peroxisome relocation-based gut-brain crosstalk. *Cell Rep.* **40**, 111140 (2022).
47. Petriv, O. I., Pilgrim, D. B., Rachubinski, R. A. & Titorenko, V. I. RNA interference of peroxisome-related genes in *C. elegans*: a new model for human peroxisomal disorders. *Physiol. Genomics* **10**, 79–91 (2002).
48. Poirier, Y., Antonenkov, V. D., Glumoff, T. & Hiltunen, J. K. Peroxisomal beta-oxidation—a metabolic pathway with multiple functions. *Biochim. Biophys. Acta* **1763**, 1413–1426 (2006).
49. He, Y. et al. A near-infrared fluorescent probe for detection of exogenous and endogenous hydrogen peroxide in vivo. *Dyes Pigments* **168**, 160–165 (2019).
50. Berman, J. R. & Kenyon, C. Germ-cell loss extends *C. elegans* life span through regulation of DAF-16 by *kri-1* and lipophilic-hormone signaling. *Cell* **124**, 1055–1068 (2006).
51. Chang, J. T., Kumsta, C., Hellman, A. B., Adams, L. M. & Hansen, M. Spatiotemporal regulation of autophagy during *Caenorhabditis elegans* aging. *Elife* **6**, e18459 (2017).
52. Lapierre, L. R. et al. The TFEB orthologue HLH-30 regulates autophagy and modulates longevity in *Caenorhabditis elegans*. *Nat. Commun.* **4**, 2267 (2013).
53. Meléndez, A. et al. Autophagy genes are essential for dauer development and life-span extension in *C. elegans*. *Science* **301**, 1387–1391 (2003).
54. Zhang, H. et al. Guidelines for monitoring autophagy in *Caenorhabditis elegans*. *Autophagy* **11**, 9–27. (2015).
55. Ruck, A. et al. The Atg6/Vps30/Beclin 1 ortholog BEC-1 mediates endocytic retrograde transport in addition to autophagy in *C. elegans*. *Autophagy* **7**, 386–400 (2011).
56. Russell, R. C. et al. ULK1 induces autophagy by phosphorylating Beclin-1 and activating VPS34 lipid kinase. *Nat. Cell Biol.* **15**, 741–750 (2013).
57. Glick, D., Barth, S. & Macleod, K. F. Autophagy: cellular and molecular mechanisms. *J. Pathol.* **221**, 3–12 (2010).
58. Kapeta, S., Chondrogianni, N. & Gonos, E. S. Nuclear erythroid factor 2-mediated proteasome activation delays senescence in human fibroblasts. *J. Biol. Chem.* **285**, 8171–8184 (2010).
59. Dimri, G. P. et al. A biomarker that identifies senescent human cells in culture and in aging skin in vivo. *Proc. Natl Acad. Sci. USA* **92**, 9363–9367 (1995).
60. Kabil, O. & Banerjee, R. Enzymology of H₂S biogenesis, decay and signaling. *Antioxid. Redox Signal.* **20**, 770–782 (2014).
61. Lee, H. J. et al. Prostaglandin signals from adult germ stem cells delay somatic aging of *Caenorhabditis elegans*. *Nat. Metab.* **1**, 790–810 (2019).
62. Bai, P. et al. PARP-1 inhibition increases mitochondrial metabolism through SIRT1 activation. *Cell Metab.* **13**, 461–468 (2011).
63. Das, A. et al. Impairment of an endothelial NAD(+)-H(2)S signaling network is a reversible cause of vascular aging. *Cell* **173**, 74–89.e20 (2018).
64. Mouchiroud, L., Houtkooper, R. H. & Auwerx, J. NAD⁺ metabolism: a therapeutic target for age-related metabolic disease. *Crit. Rev. Biochem. Mol. Biol.* **48**, 397–408 (2013).
65. Fang, E. F. et al. NAD(+) augmentation restores mitophagy and limits accelerated aging in Werner syndrome. *Nat. Commun.* **10**, 5284 (2019).
66. Hwang, P. M., Cai, F., Pineda-Sanabria, S. E., Corson, D. C. & Sykes, B. D. The cardiac-specific N-terminal region of troponin I positions the regulatory domain of troponin C. *Proc. Natl Acad. Sci. USA* **111**, 14412–14417 (2014).
67. Schieber, M. & Chandel, N. S. TOR signaling couples oxygen sensing to lifespan in *C. elegans*. *Cell Rep.* **9**, 9–15 (2014).
68. Meng, J. et al. The decay of redox-stress response capacity is a substantive characteristic of aging: revising the redox theory of aging. *Redox Biol.* **11**, 365–374 (2017).
69. Bishop, N. A. & Guarente, L. Two neurons mediate diet-restriction-induced longevity in *C. elegans*. *Nature* **447**, 545–549 (2007).
70. Tullet, J. M. A. et al. The SKN-1/Nrf2 transcription factor can protect against oxidative stress and increase lifespan in *C. elegans* by distinct mechanisms. *Aging cell* **16**, 1191–1194 (2017).

71. Pajares, M. et al. Transcription factor NFE2L2/NRF2 is a regulator of macroautophagy genes. *Autophagy* **12**, 1902–1916 (2016).
 72. Williams, D. S., Cash, A., Hamadani, L. & Diemer, T. Oxaloacetate supplementation increases lifespan in *Caenorhabditis elegans* through an AMPK/FOXO-dependent pathway. *Aging Cell* **8**, 765–768 (2009).
 73. O'Rourke, E. J., Kuballa, P., Xavier, R. & Ruvkun, G. ω -6 Polyunsaturated fatty acids extend life span through the activation of autophagy. *Genes Dev.* **27**, 429–440 (2013).
 74. Chin, R. M. et al. The metabolite α -ketoglutarate extends lifespan by inhibiting ATP synthase and TOR. *Nature* **510**, 397–401 (2014).
 75. Brenner, S. The genetics of *Caenorhabditis elegans*. *Genetics* **77**, 71–94 (1974).
 76. Kamath, R. S. & Ahringer, J. Genome-wide RNAi screening in *Caenorhabditis elegans*. *Methods* **30**, 313–321 (2003).
 77. Dennis, G. Jr. et al. DAVID: database for annotation, visualization, and integrated discovery. *Genome Biol.* **4**, P3 (2003).
 78. Ma, Y. C. et al. YAP in epithelium senses gut barrier loss to deploy defenses against pathogens. *PLoS Pathog.* **16**, e1008766 (2020).
 79. Pfaffl, M. W. A new mathematical model for relative quantification in real-time RT-PCR. *Nucleic Acids Res.* **29**, e45 (2001).
 80. Nazarko, T. Y., Farré, J. C. & Subramani, S. Peroxisome size provides insights into the function of autophagy-related proteins. *Mol. Biol. Cell* **20**, 3828–3839 (2009).
 81. Zou, C. G., Tu, Q., Niu, J., Ji, X. L. & Zhang, K. Q. The DAF-16/FOXO transcription factor functions as a regulator of epidermal innate immunity. *PLoS Pathog.* **9**, e1003660 (2013).
 82. Inoue, H. et al. The *C. elegans* p38 MAPK pathway regulates nuclear localization of the transcription factor SKN-1 in oxidative stress response. *Genes Dev.* **19**, 2278–2283 (2005).
 83. Zou, Z. et al. A single-cell transcriptomic atlas of human skin aging. *Dev. Cell* **56**, 383–397.e388 (2021).
- of Yunnan Characteristic Plant Extraction Laboratory (2022YKZY006 to C.-G.Z.).

Author contributions

C.-G.Z., N.W., and Y.-C.M. designed the experiments and analyzed the data. N.W., Y.-C.M, X.-Q.G., P.-J.Z., Y.-J.J, Q.Z., and J.-H.D performed the experiments. C.-G.Z., N.W., and Y.-C.M. interpreted the data. C.-G.Z. and Y.-C.M. wrote the manuscript.

Competing interests

The authors declare no competing interests.

Additional information

Supplementary information The online version contains supplementary material available at <https://doi.org/10.1038/s41467-023-35899-1>.

Correspondence and requests for materials should be addressed to Cheng-Gang Zou.

Peer review information *Nature Communications* thanks Konstantinos Palikaras and the other, anonymous, reviewer(s) for their contribution to the peer review of this work.

Reprints and permissions information is available at <http://www.nature.com/reprints>

Publisher's note Springer Nature remains neutral with regard to jurisdictional claims in published maps and institutional affiliations.

Open Access This article is licensed under a Creative Commons Attribution 4.0 International License, which permits use, sharing, adaptation, distribution and reproduction in any medium or format, as long as you give appropriate credit to the original author(s) and the source, provide a link to the Creative Commons license, and indicate if changes were made. The images or other third party material in this article are included in the article's Creative Commons license, unless indicated otherwise in a credit line to the material. If material is not included in the article's Creative Commons license and your intended use is not permitted by statutory regulation or exceeds the permitted use, you will need to obtain permission directly from the copyright holder. To view a copy of this license, visit <http://creativecommons.org/licenses/by/4.0/>.

© The Author(s) 2023

Acknowledgements

We are grateful to Dr. Jianping Xu (McMaster University, Canada) for his critical reading of this manuscript. We thank the *Caenorhabditis* Genetics Center, Drs. B Liang, B Qi, MQ Dong, H Zhang, and H Zhu for nematode strains, and Dr. X Zhao for IMR90 cells. Some nematode strains were kindly provided by the *Caenorhabditis* Genetics Centre, which is funded by the NIH Office of Research Infrastructure Programs (P40 ODO10440). This work was supported by a grant from the National Natural Science Foundation of China (32170759 to C.-G.Z.), the Major Science and Technology Project in Yunnan Province of China (202001BB050001 to C.-G.Z.), and the independent research fund